ISSN 0020-1685, Inorganic Materials, 2018, Vol. 54, No. 2, pp. 125–132. © Pleiades Publishing, Ltd., 2018.
Original Russian Text © E.V. Dedyaeva, D.V. Zaitsev, E.A. Lukina, P.N. Nikiforov, A.G. Padalko, G.V. Talanova, K.A. Solntsev, 2018, published in Neorganicheskie Materialy, 2018, Vol. 54, No. 2, pp. 138–145.

Effect of Barothermal Processing on the Solid-State Formation of the Structure and Properties of 16 at % Si–Al Hypereutectic Alloy

E. V. Dedyaeva[a], D. V. Zaitsev[b], E. A. Lukina[b], P. N. Nikiforov[c], A. G. Padalko[a, *], G. V. Talanova[a], and K. A. Solntsev[a]

[a] *Baikov Institute of Metallurgy and Materials Science, Russian Academy of Sciences, Leninskii pr. 49, Moscow, 119334 Russia*
[b] *All-Russia Research Institute of Aviation Materials (Russian Federation State Scientific Center), ul. Radio 17, Moscow, 105005 Russia*
[c] *Ufa Engine Industrial Association Public Joint Stock Company, ul. Ferina 2, Ufa, 450039 Russia*
**e-mail: padalko@inbox.ru*

Received March 21, 2017; in final form, June 23, 2017

Abstract—We describe barothermal processing (hot isostatic pressing) of a 16 at % Si–Al binary alloy for 3 h at a temperature of 560°C and pressure of 100 MPa for 3 h, in combination with measurements of heat effects during cooling. The results demonstrate that this processing leads to the fragmentation of the silicon structural constituent and ensures a high degree of homogenization of the as-prepared alloy. Heat treatment of the 16 at % Si–Al alloy at 560°C and a pressure of 100 MPa leads to a thermodynamically driven enhanced silicon dissolution, up to ~10 at %, in the aluminum matrix, resulting in the formation of a supersaturated solid solution, which subsequently decomposes during cooling. We analyze the complete porosity elimination process, which makes it possible to obtain a material with 100% relative density. According to differential barothermal analysis, microstructural analysis, and scanning and transmission electron microscopy data, barothermal processing of the 16 at % Si–Al alloy produces a bimodal size distribution of the silicon phase constituent: microparticles 3.6 μm in average size and nanoparticles down to ~1 nm in diameter. The Al matrix has been shown to contain a high density of edge dislocations. Barothermal processing reduces the thermal expansion coefficient and microhardness of the hypereutectic alloy. We conclude that solid-state barothermal processing is an effective tool for completely eliminating microporosity from the 16 at % Si–Al alloy, reaching a high degree of homogenization, and controlling the microstructure of the alloy, in particular by producing high dislocation density in the aluminum matrix.

Keywords: hot isostatic pressing, silumins, silicon microparticles, dislocations

DOI: 10.1134/S0020168518020024

INTRODUCTION

Aluminum alloys are widely used in modern technology to produce structural materials with low density, high corrosion resistance, and rather good mechanical properties. Alloys based on the simple eutectic binary system Al–Si constitute a considerable fraction of the aluminum-based metallic materials. Since a large amount of reliable experimental data obtained in physicochemical studies was used to construct the equilibrium phase diagram of this system [1], it is considered canonical [2, 3]. The system is distinctive in that there is no chemical interaction between the components of the alloy over the entire composition range. It contains a rather wide range of solid solutions of silicon in aluminum (Al), with a solubility limit of ~1.6 at % Si at the eutectic temperature (577°C, 12.2 at % Si) [1–3]. In addition, the binary alloys of the Al–Si system have the advantages of being easy to synthesize, having relatively low phase transformation temperatures, being composed of components with low saturated vapor pressure, and being nonreactive with typical crucible materials, which allows these alloys to be employed as model systems for gaining insight into barothermal processing mechanisms.

Cast aluminum alloys based on the basic binary system Al–Si (silumins) constitute a large group of materials containing 7–12 at % silicon. Silicon-rich silumins, containing more than 12 at % silicon, are of little or no use in structural applications, but given that their thermal expansion coefficient (TEC) decreases linearly with increasing silicon content, attention has also been paid to silicon-rich alloys with reduced TECs. To improve their mechanical properties, cast silumins are heat-treated with the aim of reducing the cooling-induced stress in the cast alloys and improving the morphology of the coarse needle-like (α + Si) eutectic present in the cast material and unfavorable for its mechanical properties [4]. In silumins intended for use in highly loaded parts, shrinkage porosity is eliminated by hot isostatic pressing (HIP) [5, 6]. Heating a material in order to reduce its yield strength,

in combination with uniform pressure applied, makes it possible to considerably raise the density of the material, often to its theoretical density, thereby improving its mechanical and engineering characteristics [6]. This technique relies, on the one hand, on a theoretical basis that allows one to model HIP densification processes [7–9] and, on the other, on dilatometric studies of densification processes [10, 11]. A number of studies have been concentrated on the HIP of aluminum alloys for the fabrication of high-density materials [12, 13]. At the same time, there has been much less work on phenomena related to barothermal processing (BTP) induced changes in the morphology of structural constituents of alloys.

In connection with this, the purpose of this work was to assess the effect of BTP on solid-state microstructure formation in 16Si–Al binary alloy and find correlation between its structural parameters and some of its mechanical properties.

EXPERIMENTAL

16Si–Al alloy samples for this investigation were synthesized through melting PA-1 aluminum powder (≥99% Al) with a particle size under 100 μm and Kr00 silicon powder (≥99% Si) with a similar particle size composition. Ingots were prepared by vacuum suction using a Kristall-702 inductively heated system in flowing argon. After melting the powders, the melt was heated in a quartz crucible to 700°C, which was 50°C above the liquidus temperature for the composition in question. After complete silicon dissolution in the aluminum, a quartz tube 3.6 mm in inner diameter was immersed vertically in the melt. After the pressure in the tube was sharply reduced relative to that in the melt, the liquid metal filled the tube to a height on the order of 100 mm. Under these conditions, the melt was then cooled at a rate on the order of tens of degrees Celsius, with supercooling. These synthesis conditions resulted in multinucleus crystallization and the formation of samples with a microcrystalline structure and a rather uniform distribution of the structural components of the alloy: aluminum and silicon. For experiments requiring larger samples, we performed standard syntheses: ingots 15 mm in diameter and 80 mm in length were produced by melt casting into graphite–fireclay molds.

BTP was carried out in an HIRP 20/70-200-2000 apparatus (ABRA, Switzerland) in an argon atmosphere using a system of graphite heaters. After the samples were placed in the working chamber, the pressure was raised to ~53 MPa and then the temperature was raised at a constant rate of 10°C/min. At the required temperature, the pressure reached 100 ± 2 MPa. This temperature was maintained with an accuracy of ±1°C throughout the holding time. After the barothermal processing cycle, the samples were cooled to 300°C at a rate of 7°C/min and then to room temperature at a higher rate.

Samples for characterization, 3.6 mm in diameter and ~3–10 mm in height, were prepared using a diamond saw blade, diamond pastes, electrolytic polishing, and chemical etching. Microstructures were examined on an MeF3 optical microscope (Austria), by scanning electron microscopy (SEM) on a TESCAN VEGA SBU 11 instrument (Czechia), and by transmission electron microscopy on a Tecnai G2 F20 instrument. X-ray diffraction measurements were made on a Shimadzu XRD-6000 diffractometer (Japan) with CuK_α radiation. Vickers microhardness tests were performed on a PMT-3 microhardness tester (OAO LOMO, Russia). The linear thermal expansion of the samples was measured on a DIL 402 C dilatometer (Netzsch, Germany) equipped with a vacuum furnace. Quantitative information about the microstructural constituents of the alloy was obtained by processing and analyzing images and data arrays using appropriate software, including ImageJ.

RESULTS AND DISCUSSION

The microstructure of the as-prepared alloy (Fig. 1a) consisted of coarse primary silicon crystals and needle-like eutectic silicon microcrystals up to 40–50 μm in length, with a cross-sectional size on the order of a few microns, which formed an essentially continuous silicon skeleton in the aluminum matrix. The synthesized as-prepared alloy had considerable porosity, localized in the α-matrix, whereas the primary and eutectic silicon crystals and needles were free of such structural defects. By analyzing optical microscopy images with the use of appropriate software, we obtained a histogram of the pore size distribution (Fig. 1b) and quantitative data on the porosity of the as-prepared material. In particular, porosity characteristics were as follows: the pore volume fraction in the α-matrix was 6.0 vol % as determined proceeding from quantitative metallography [14], the pore number density was 4.7×10^9 cm^{-3}, the average center-to-center pore distance was 6.0 μm, the average pore diameter was 0.75 μm, and the average pore volume was 2.2×10^{-13} cm^3. The reason for the increased porosity of the as-prepared material was that the alloy was synthesized from powders. Since the aluminum and silicon particles had surface oxide films, this led to pore formation.

The BTP temperature was chosen using previously reported differential barothermal analysis (DBA) data [15], which showed that, at a pressure of 100 MPa, heating the 16Si–Al alloy led to solid-state silicon dissolution at a temperature of ~550°C and that subsequent cooling led to the precipitation of silicon micro- and nanoparticles as a result of the decomposition of the supersaturated (Al) solid solution. Based on those results, small ingots 3.6 mm in diameter and 10 mm in length were subjected to BTP for 3 h at an isobaric–isothermal holding temperature of 560 ± 1°C, which

was ~10°C above the solid-state transformation temperature according to DBA data.

SEM examination showed that the microstructure of the alloy underwent significant changes (Fig. 2a). First, the as-prepared, porous alloy acquired a total density. Microstructural defects in the form of pores in the aluminum-based solid solution were detected at none of the magnifications used in optical microscopy or SEM (up to 27000×). This result is sufficiently obvious because the applied uniform pressure of 100 MPa considerably exceeds the yield strength of the alloy containing 0.72 wt % silicon: ~10 MPa at a temperature of 500°C, as determined from uniaxial compression results obtained in the temperature range 30–500°C [16]. Subsequently, we assumed that a major contribution to the yield strength was made by the aluminum structural constituent and that, with increasing silicon concentration in the alloy, it increased but remained on the same order. When extrapolating the data obtained by Schumacher et al. [16] to higher BTP temperatures, it is reasonable to expect a decrease in the yield strength of the aluminum matrix of the 16Si–Al alloy at 560°C to a few megapascals. The applied uniform pressure of 100 MPa is then many times higher than the yield strength of the alloy and plays a key role in determining active plastic deformation of the pores, subsequent closure of their walls, and diffusion joining of the surfaces brought into contact. In analyzing the diffusion joining process, we proceeded from the temperature dependence obtained by Fujikawa et al. [17] for the self-diffusion coefficient of aluminum atoms under ordinary conditions and assumed that, at the pressure of 100 MPa used in this study, only a slight pressure-induced decrease in aluminum self-diffusion coefficient is possible, by analogy with previous results on the influence of pressure on diffusion coefficients in high-temperature nickel alloys ($D^{100\ \mathrm{MPa}} \sim 0.9D^{0.1\ \mathrm{MPa}}$) [18]. Using the temperature dependence of the aluminum self-diffusion coefficient [17], we find that, according to the Einstein equation $l^{833}_{\mathrm{Al}/\mathrm{Al}} = (D^{833}_{\mathrm{Al}/\mathrm{Al}}\tau)^{1/2}$, the diffusion distance of aluminum atoms at 560°C during the isobaric–isothermal holding time (10800 s) reaches 80 μm [19]. Therefore, the pore walls brought into contact by a plastic deformation mechanism in the aluminum matrix during BTP completely consolidate, which determines the total density of the alloy.

Significant changes were also observed in the morphology of the silicon microparticles (Fig. 2a). BTP converted the coarse, needle-like shape of the starting eutectic silicon inclusions into a uniform microstructure with fragmented silicon particles, whereas the morphology of the primary silicon crystals remained essentially unchanged. Therefore, the BTO process was accompanied by active silicon dissolution in the aluminum, which led to a high degree of homogenization of the alloy. This circumstance is due to the thermodynamically driven silicon dissolution in the aluminum under applied uniform pressure, which leads to a reduction in the lattice parameter of the aluminum-based solid solution [1] and to a reduction in its specific volume, thermodynamically preferred at high pressures. An increase in silicon solubility in aluminum (up to 15 at %) at high pressures was also reported by Mii et al. [20]. Thus, as a result of barothermal processing of the 16Si–Al alloy, an increased amount of silicon can dissolve in the aluminum matrix, considerably exceeding the equilibrium value 1.38 at % in the phase diagram of the Al–Si system [1–3]. This model is supported by the morphology of the silicon particles (Fig. 2a), which can be divided into two types. The particles of one type are rounded in shape and have a length-to-width ratio on the order of unity. The parti-

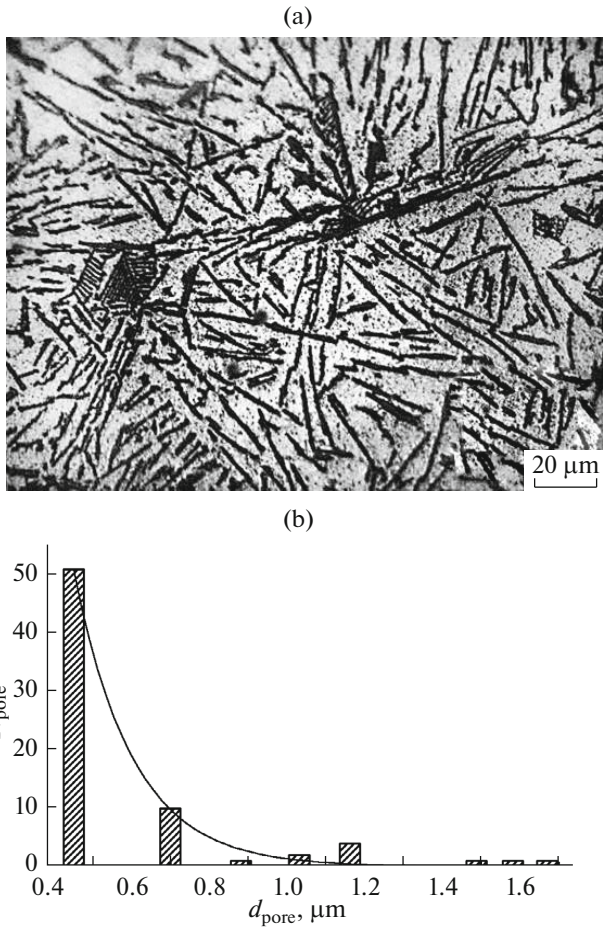

Fig. 1. (a) Microstructure of the as-prepared 16Si–Al alloy (optical microscopy; magnification, 500×; image dimensions, 150 × 200 μm), consisting of coarse primary silicon crystals, a needle-like Al + Si eutectic, and pores in the aluminum matrix; (b) histogram of the pore size distribution in the aluminum matrix of the as-prepared alloy, which can be represented by the relation $N^0_{\mathrm{pore}} = 1.0 \times 10^3 e^{-6.7 d_{\mathrm{pore}}}$, where N^0_{pore} is the number of pores in the starting material and d_{pore} is the pore diameter.

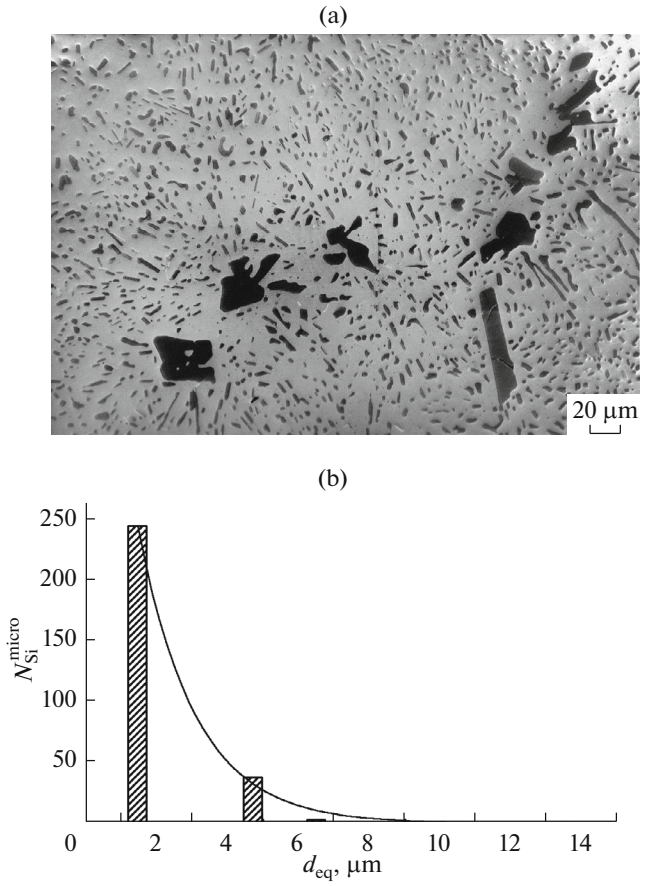

Fig. 2. (a) Microstructure of the 16Si–Al alloy (SEM) containing bulk primary silicon particles after BTP at 100 MPa and 560°C for 3 h (1000×; image dimensions, 270 × 385 μm); (b) histogram of the size distribution of the silicon microparticles (except the primary crystals) in the 16Si–Al alloy after BTP.

cles of the other type have an elongated morphology, with a length-to-width ratio ranging from 2 to ~20. Under the assumption that the rounded particles were formed as a result of dissolution and subsequent precipitation on cooling and that the elongated particles were the undissolved residues of the eutectic silicon needles, it follows from a semiquantitative estimate of the relationship between the rounded and elongated particles that the fraction of precipitates in the supersaturated (Al) solid solution is on the order of 8–10 vol %. This means that, at an overall silicon content of 16 at %, on the order of 8–10 at % silicon was dissolved in the course of BTP, which considerably exceeds the silicon solubility limit in aluminum under ordinary conditions [1–3].

Figure 3 shows a DBA curve of the alloy. The insignificant height of the exothermic peak (~3% of the height of the high-pressure crystallization peak of the alloy [15]) obtained upon the decomposition of the (Al) solid solution correlates with results reported by Schumacher et al. [16] on silicon precipitation from a

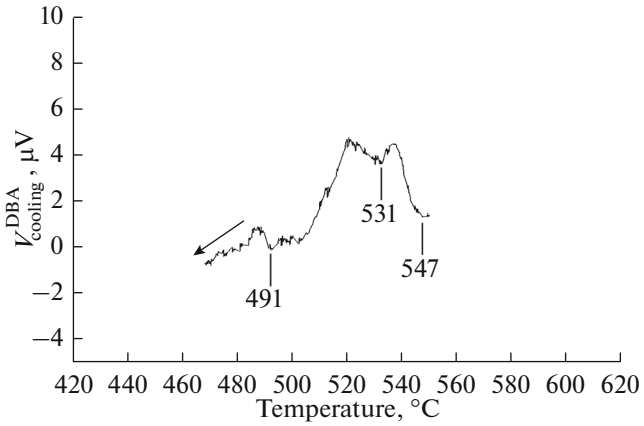

Fig. 3. Portion of a DBA cooling curve of the 16Si–Al alloy after exposure to a temperature of 560°C and pressure of 100 MPa for 3 h.

supersaturated (Al) solid solution under ordinary conditions. The curve indicates that, after the exposure of the alloy to 560°C and 100 MPa, silicon precipitation from the solid solution begins at 547°C, which agrees well with previously reported data (550°C) [15]. The composite nature of the peak can be accounted for in terms of stages in the decomposition of the (Al) solid solution. The initial stage is the growth of the undissolved silicon particles. The next stage, at 531°C, is the nucleation and growth of silicon microparticles in the aluminum matrix. This process reaches completion at 520°C, and starting at 491°C we observe the precipitation of nanoparticles.

The silicon microcrystals are rather evenly distributed over the aluminum matrix, without predominant localization. To interpret this experimental finding, we took into account the temperature dependence of the equilibrium diffusion coefficient of silicon in aluminum under ordinary conditions [17], assuming that a uniform pressure of 100 MPa reduces it only slightly and that, accordingly, the diffusion distance of the silicon atoms reaches 80 μm [19]. Therefore, the silicon atoms can be sufficiently evenly distributed over the alloy, including the axes of aluminum dendrites. This model agrees well with the present SEM data (Fig. 2a). Quantitative information about the silicon phase constituent of the 16Si–Al alloy after the BTP cycle is presented in Fig. 2b in the form of a histogram of the size distribution of the silicon microparticles. It is seen that the particle size distribution is well fitted by the exponential relation $N_{Si}^{micro} = 6.0 \times 10^2 e^{-0.6 d_{eq}}$, where N_{Si}^{micro} is the number of silicon microparticles and d_{eq} is the equivalent diameter of a silicon microparticle. From this distribution, the average equivalent diameter of the silicon particles was determined to be 3.6 ± 0.3 μm, and the average particle volume, 2.4×10^{-11} cm^3. Their volume fraction evaluated from the total area occupied by the silicon phase [14] was 14.2 ± 1.5 vol %. The surface

and volume microparticle concentrations were 1.1×10^6 cm^{-2} and 1.2×10^9 cm^{-3}, respectively. At this surface particle concentration, the average center-to-center distance between the particles was 9.5 μm. Note that the overall content of silicon microparticles in the alloy, as determined by quantitative microstructural analysis, is lower than the nominal silicon content (16 at %). This circumstance is related to the instrumental capabilities of quantitative microstructural analysis, which were unsuitable for gaining information about micro- and nanoparticles in a single SEM image. To assess BTP efficiency, we present quantitative data on the microstructure of the commercially available silumin AK7pch, containing 7 at % silicon, after standard heat treatment [21], in which the phase constituents at a surface density of 4.9×10^5 cm^{-2} had an average size of 5.6 μm and an average center-to-center distance of 15.6 μm. These parameters differ markedly from the quantitative characteristics of the silicon structural constituent in the 16Si–Al alloy after a BTP cycle.

To obtain a more detailed information about the particle size of the silicon phase constituent, we used SEM at higher magnifications, up to 27000× (Fig. 4). The image in Fig. 4 shows a twinned silicon particle that was formed, according to Shamsuzzoha and Hogan [22] during the solidification of a synthesized alloy. It is that the aluminum matrix contains a considerable concentration of much finer silicon particles, ~40–100 nm in diameter.

Assuming that the size of some silicon nanoparticles may be below the resolving power of standard SEM, we used TEM. The TEM image in Fig. 5 demonstrates the presence of a dense disordered dislocation network in the aluminum matrix. The silicon microparticle in Fig. 5a, which was, most likely, formed as a result of the decomposition of the supersaturated (Al) solid solution, has a twinned structure. The dark-field image of a portion of the matrix in Fig. 5b has contrast characteristic of fine coherent particles. A quantitative assessment of the particles, with allowance for the fact that the TEM image was obtained from an entire 80-nm-thick foil, showed that the particles had a rather high number density, on the order of 2.7×10^{11} cm^{-2}, which approaches the limiting dislocation density in metals after deformation processing. Following an approach that made it possible to obtain reliable information about β'' nanoprecipitates in an alloy of the Al–Mg–Si system [23], we Fourier transformed the image. The results are presented in Fig. 5c. The [111] crystallographic direction lies in the plane of the foil, and the image shows (111) Al atomic planes. It is seen that the *a* and *b* planes, typical of the image under consideration, are discontinuous, and a *c* plane then emerges in the same direction, which corresponds to an edge dislocation [24]. A similar picture was observed in a TEM image of plastically deformed zirconium [25]. Edge dislocations, detected by TEM, act as sites of preferential precipitation of silicon particles during the decomposition of the (Al) solid solution (Fig. 5c), resulting in the formation of an edge dislocation–silicon nanoparticle pair, which leads to the same high concentration of silicon nanoparticles. The present results regarding the presence of nanoparticles in the 16Si–Al alloy are consistent with data reported by Schumacher et al. [16], who demonstrated, using atom probe tomography, the formation of silicon nanoparticles for two hypoeutectic alloys of the Al–Si system in the region of solid solutions containing ≤0.72 at % silicon. They examined silicon precipitation at normal pressure after annealing above the solvus temperature in the alloys at slow cooling rates (down to 0.001 K/s).

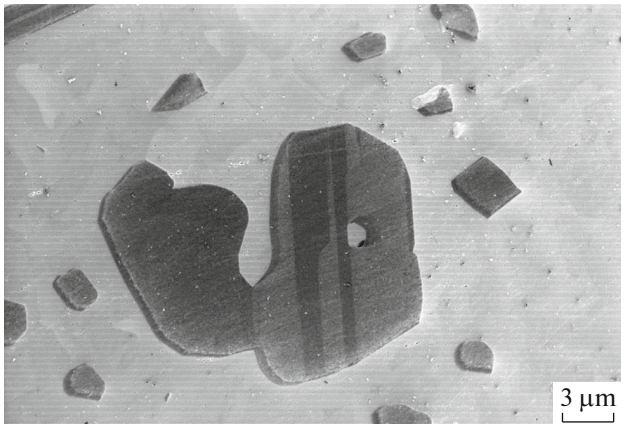

Fig. 4. Fragments of primary silicon crystals and silicon micro- and nanoparticles formed in the aluminum matrix as a result of the decomposition of the supersaturated (Al) solid solution during the BTP of the 16Si–Al alloy.

The X-ray diffraction pattern of the 16Si–Al alloy after BTP showed only reflections from aluminum and silicon phases (Fig. 6a). In the diffraction pattern obtained, we analyzed all five peaks of Al (*hkl*) and five peaks of Si (*hkl*), separating the K_{α_1} components and finding its peak position in order to determine the lattice parameters of the aluminum and silicon (Fig. 6b). It follows from the decomposition results for all five peaks of silicon that BTP increases the lattice parameter of the silicon structural constituent, consisting of micro- and nanoparticles, to $a_{Si}^{BTP} = 5.439 \pm 0.003$ Å in comparison with the lattice parameter of pure silicon powder prepared by the same technique ($a_{Si} = 5.431 \pm 0.003$ Å). The increase may be due to the partial distortion of the crystal lattice of the Si nanoparticles upon precipitation from the (Al) solid solution. In addition, BTP increased the lattice parameter of the aluminum matrix (evaluated from the position of five peaks) to 4.054 ± 0.002 Å in comparison with $a_{Al} = 4.049 \pm 0.002$ Å, which may be due to the high density of edge dislocations in the α-matrix: local lattice dis-

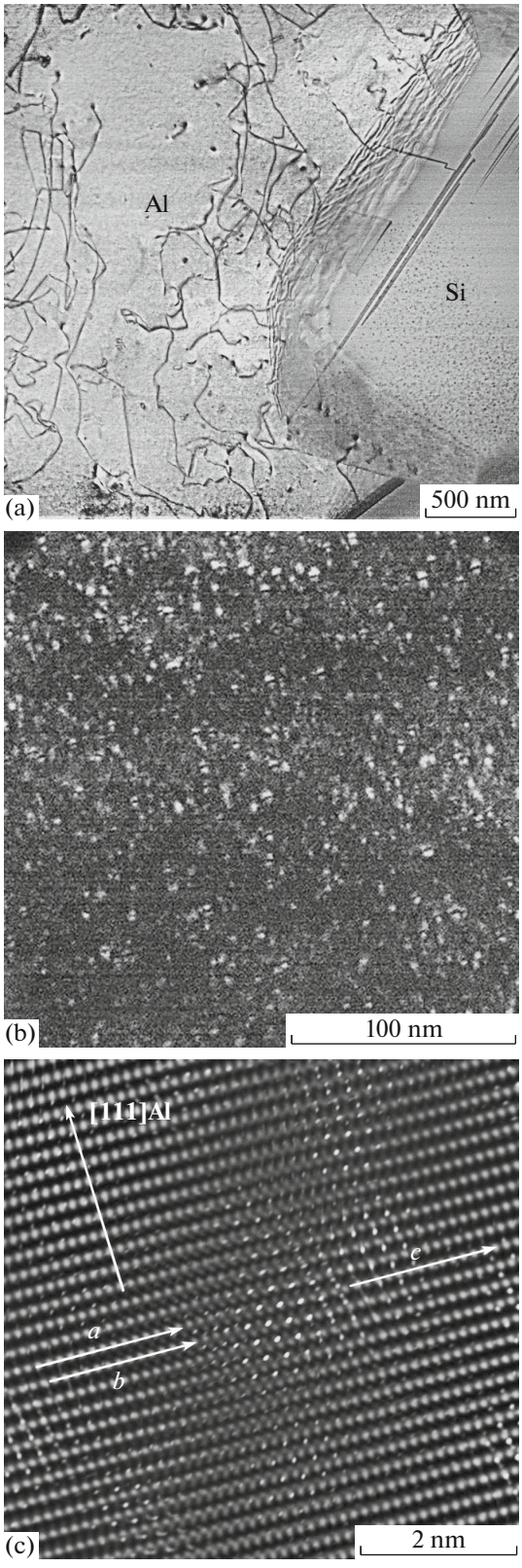

Fig. 5. TEM results for the 16Si–Al binary alloys after BTP at 100 MPa and 560°C for 2 h: (a) bright-field image of the Al matrix (with dislocations) and a Si particle, (b) dark-field image (**g** = (111), ⟨112⟩ zone axis) of the Al matrix with a characteristic contrast of fine coherent inclusions, (c) edge dislocation–silicon nanoparticle complex.

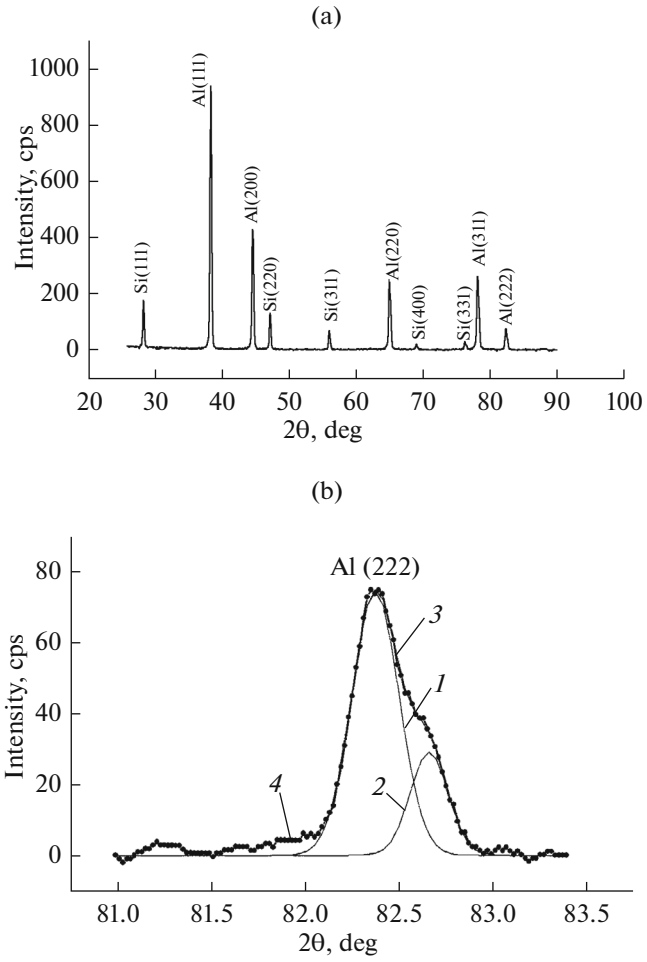

Fig. 6. X-ray diffraction characterization results: (a) X-ray powder diffraction pattern of the 16Si–Al alloy after BTP, (b) typical decomposition results exemplified by the Al (222) peak: (*1*) CuK_{α_1} component of the peak, (*2*) CuK_{α_2} component of the peak, (*3*) superposition of peaks *1* and *2*, (*4*) composite peak.

order in the dislocations leads to a slight increase in lattice parameter.

According to thermal expansion coefficient (TEC) measurements, the average TEC of the as-prepared alloy in the temperature range 70–150°C, $\alpha_0^{70-150} = 19.5 \times 10^{-6}$ K^{-1}, correlates with the average TEC of the heat-treated 16Si–Al alloy in the temperature range 20–100°C: $\alpha_{av}^{20-100} = 19.9 \times 10^{-6}$ K^{-1} [26]. A BTP cycle shifts the curve representing the temperature dependence of the TEC (Fig. 7) to lower values, and the average TEC decreases to $\alpha_{BTP}^{20-100} = 17.5 \times 10^{-6}$ K^{-1}, which is lower than that reported by Hidnert and Krider [26] for the 16Si–Al alloy: 19.9×10^{-6} K^{-1}. The relative BTP-induced decrease in TEC is ~12% relative to the as-prepared alloy, which is due, first, to the removal of microporosity, an additional factor raising

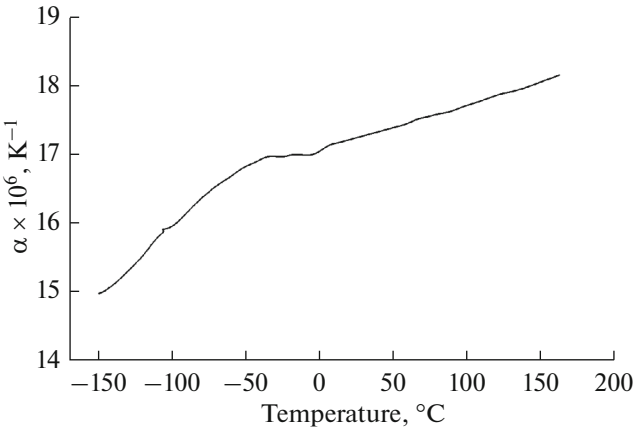

Fig. 7. Temperature dependence of the TEC for the 16Si–Al alloy after BTP.

the TEC, and, second, to the partial disordering of the crystal lattice of the nanoscale silicon phase constituent of the alloy, as well as to the high defect density in the crystal lattice of the aluminum, which also leads to a reduction in the TEC of the alloy.

The Vickers microhardness of the alloy after BTP was determined by indenting the two-phase material. Note that an indent ~800 μm^2 in area covered on the order of 9 microparticles, up to 2.2 × 10^6 silicon nanoparticles, and more than 2.2 × 10^6 dislocations (with allowance for the TEM results). The high dislocation density considerably reduced microhardness, to 366 ± 11.6 MPa. This is markedly lower than the measured microhardness of the as-prepared alloy (601 MPa), which correlates well with the microhardness of a number of commercially available silumins [27].

CONCLUSIONS

Exposure of the 16Si–Al binary alloy to a temperature of 560°C and a pressure of 100 MPa gives rise to active diffusion processes, which make it possible to significantly fragment the needle-like eutectic silicon crystals and markedly improve the homogeneity of the as-prepared alloy, which is chemically and structurally inhomogeneous.

The morphology of the silicon microparticles in the 16Si–Al alloy attests to a thermodynamically driven enhanced silicon dissolution, up to ~10 at %, in the aluminum matrix during heating, resulting in the formation of a supersaturated solid solution, which subsequently decomposes during cooling.

An applied uniform pressure of 100 MPa is many times higher than the yield strength of the alloy at 560°C and plays a key role in determining plastic deformation of pores, closure of their walls, and subsequent diffusion joining of the surfaces brought into contact, enabling one to produce a material with 100% relative density.

A high uniform pressure leads to edge dislocation generation in the α-matrix—up to a density of 2.7 × 10^{11} cm^{-2}, which approaches the limiting dislocation density in metals—and to the formation of edge dislocation–silicon nanoparticle complexes during subsequent silicon precipitation from the supersaturated (Al) solid solution.

According to the present DBA, microstructural analysis, SEM, TEM, and X-ray diffraction data, BTP of the 16Si–Al alloy produces a bimodal size distribution of the silicon phase constituent: microparticles 3.6 μm in average size and nanoparticles down to ~1 nm in diameter. The bimodal microstructure obtained and the high density of structural defects in the aluminum matrix reduce the microhardness of the alloy.

Solid-state BTP is an effective tool for completely eliminating microporosity in the Al–16Si alloy, reaching a high degree of homogenization, and producing a near-optimal microstructure, and allows one to significantly change the perfection of the aluminum matrix, which is comparable to and surpasses results of conventional heat treatment of the material at atmospheric and reduced pressures.

REFERENCES

1. Murray, J.L. and McAlister, A.J., The Al–Si (aluminum–silicon) system, *Bull. Alloy Phase Diagrams,* 1984, vol. 5, pp. 74–84.
2. Hansen, M. and Anderko, K., *Constitution of Binary Alloys,* New York: McGraw-Hill, 1958, 2nd ed., vols. 1–2.
3. *Diagrammy sostoyaniya dvoinykh metallicheskikh sistem* (Phase Diagrams of Binary Metallic Systems), 3 vols., Lyakishev, N.P., Ed., Moscow: Mashinostroenie, 1996, 1997, 2001.
4. *Aluminum and Its Alloys. Effect of Silicon on Silumins.* http://cdn-as3.myvirtualpaper.com/s/soedinitel/aliegosplavy/2011053101/upload/aliegosplavy.pdf.
5. Ceschini, L., Morri, A., and Sambogna, G., The effect of hot isostatic pressing on the fatigue behavior of sand-cast A356-T6 and A204-T6 aluminum alloys, *J. Mater. Process. Technol.,* 2008, vol. 204, pp. 231–238.
6. Chama, C.C., Distribution of Al 332 12Fe3Si and ($FeAl_6$)Si in a hiped Al–10.71 wt% Si casting, *Mater. Character.,* 1996, vol. 37, no. 4, pp. 177–181.
7. Bouvard, D. and Ouedraogo, E., Modeling of hot isostatic pressing: a new formulation using random variables, *Acta Metall.,* 1987, vol. 35, no. 7, pp. 2323–2328.
8. Li, E.K.H. and Funkenbusch, P.D., Modeling of the densification rates of monosized and bimodal-sized particle systems during hot isostatic pressing (HIP), *Acta Metall.,* 1989, vol. 37, no. 6, pp. 1645–1655.
9. Nair, S.V. and Tien, J.K., Densification mechanism map for hot isostatic pressing (HIP) of unequal sized particles, *Metall. Trans. A,* 1987, vol. 18, pp. 97–107.
10. Li, W.-B., Ashby, M.F., and Easterling, K.E., On densification and shape change during hot isostatic pressing, *Acta Metall.,* 1987, vol. 35, no. 12, pp. 2831–2842.

11. Wadley, H.N.G., Schaefer, R.J., Kahn, A.H., Ashby, M.F., Clough, R.B., Geffen, Y., and Wlassich, J.J., Sensing and modeling of the hot isostatic pressing of copper pressing, *Acta Metall. Mater.,* 1991, vol. 39, no. 5, pp. 979–986.

12. Shrinivasan, R. and Weiss, I., Formation of surface depressions during hot isostatic pressing (HIP), *Scr. Metall. Mater.,* 1990, vol. 24, pp. 2413–2418.

13. Zulfia, A., Atkinson, H.V., Jones, H., and King, S., Effect of hot isostatic pressing on cast A357 aluminum alloy with and without SiC particle reinforcement, *J. Mater. Sci.,* 1999, vol. 34, pp. 4305–4310.

14. Saltykov, S.A., *Stereometricheskaya metallografiya* (Stereometric Metallography), Moscow: Metallurgiya, 1976.

15. Dedyaeva, E.V., Akopyan, T.K., Padalko, A.G., and Fedotov, V.T., Barothermal analysis of the phase transformations and structure of Al–16 at % Si hypereutectic alloy, *Izv. Vyssh. Uchebn. Zaved., Tsvetn. Met.,* 2014, no. 7, pp. 76–79.

16. Schumacher, P., Reich, M., Mohles, V., Pogatscher, S., Uggowitzer, P.J., and Milkereit, B., Correlation between supersaturation of solid solution and mechanical behaviour of two binary Al–Si alloys, *Mater. Sci. Forum,* 2014, vols. 794–796, pp. 508–514.

17. Fujikava, S.-I., Hirano, K.-I., and Fukushima, Y., Diffusion of silicon in aluminum, *Metall. Trans. A,* 1978, vol. 9, pp. 1811–1815.

18. Beresnev, A.G., Razumovskii, I.M., Marinin, S.F., Tikhonov, A.A., and Butrim, V.N., Technological principles underlying the hot isostatic pressing of monocrystalline blades from high-temperature nickel alloys for aero engines, *Tsvetn. Met.,* 2011, no. 12, pp. 84–88.

19. Dedyaeva, E.V., Nikiforov, P.N., Padalko, A.G., Talanova, G.V., and Shvorneva, L.I., Effect of barothermal processing on the microstructure and properties of Al–10 at % Si hypoeutectic binary alloy, *Inorg. Mater.,* 2016, vol. 52, no. 7, pp. 721–728.

20. Mii, H., Senoo, M., and Fujishiro, I., Solid solubility of Si in Al under high pressure, *Jpn. J. Appl. Phys.,* 1976, vol. 15, pp. 777–783.

21. Belov, N.A., *Fazovyi sostav promyshlennykh i perspektivnykh alyuminievykh splavov* (Phase Composition of Commercially Available and Promising Aluminum Alloys), Moscow: Izd. Dom Mosk. Inst. Stali i Splavov, 2010.

22. Shamsuzzoha, M. and Hogan, L.M., The twinned growth of silicon in chill-modified Al–Si eutectic, *J. Cryst. Growth,* 1987, vol. 82, pp. 598–610.

23. Mortsell, E., Andersen, S., Marioara, C., Royset, J., Friis, J., and Holmestad, R., Characterization of multicomponent Al alloys by TEM, HAADF-STEM, EELS, *Proc. 16th Eur. Microscopy Congr.,* Lyon, 2016, pp. 209–210.

24. *Physical Metallurgy,* Cahn, R.W., Ed., Amsterdam: North-Holland, 1965.

25. Zhilyaev, A.P., Gálvez, F., Sharafutdinov, A., and Pérez-Prado, M.T., Influence of the high pressure torsion die geometry on the allotropic phase transformations in pure Zr, *Mater. Sci. Eng., A,* 2010, vol. 527, pp. 3918–3928.

26. Hidnert, P. and Krider, H.S., Thermal expansion of aluminum and some aluminum alloys, *J. Res. Natl. Bur. Stand.,* 1952, vol. 48, no. 3, pp. 209–220.

27. Prigunova, A.G., Belov, N.A., Taran, Yu.N., Zolotorevskii, V.S., Napalkov, V.I., and Petrov, S.S., *Siluminy. Atlas mikrostruktur i fraktogramm promyshlennykh splavov* (Silumins: Atlas of Microstructures and Fracture Surface Maps for Industrial Alloys), Moscow: Mosk. Inst. Stali i Splavov, 1996.

Translated by O. Tsarev